

Electronic Supplementary Information

The influence of *ortho*-methyl substitution in organometallic self-assembly – a comparative study on Cu(111) vs. Ag(111)

Massimo Fritton^{a,b}, Katrin Otte^c, Jonas Björk^d, Pronay Kumar Biswas^e, Wolfgang M. Heckl^{a,b}, Michael Schmittel^e, and Markus Lackinger^{a,b*}

^a Deutsches Museum, Museumsinsel 1, 80538 Munich, Germany

^b Department of Physics, Technische Universität München, James-Frank-Str. 1, 85748 Garching, Germany

^c Leibniz Supercomputing Centre of the Bavarian Academy of Sciences and Humanities, Boltzmannstraße 1, 85748 Garching, Germany

^d Department of Physics, Chemistry and Biology, IFM, Linköping University, 581 83 Linköping, Sweden

^e Center of Micro- and Nanochemistry and Engineering, Organische Chemie I, Universität Siegen, Adolf-Reichwein-Str. 2, 57068 Siegen, Germany

Email: markus@lackinger.org

Experimental details:

All experiments were carried out under ultra-high vacuum conditions with a base pressure below 3×10^{-10} mbar. Cu(111) and Ag(111) single crystal surfaces were prepared by cycles of Ne⁺ sputtering at 2.0 keV and radiative annealing to 500 °C. Prior to deposition of 1,3,5-tris(4-bromo-3,5-dimethylphenyl)benzene (**1**) or 1,3,5-tris(*p*-bromophenyl)benzene (**2**), the cleanliness and appropriateness of terrace sizes were verified by large scale STM images. **1** was synthesized as further described below, **2** was purchased from Sigma-Aldrich with a purity of 97%. Both molecules were deposited from home-built Knudsen cells, using the integrated quartz crystal microbalance as rate monitor.¹ A crucible temperature of 200 °C was used for sublimation of **1** and of 120 °C for **2**, respectively. All thermal sample treatments were carried out with the same heater, using identical heating and cooling rates of 1.0 °C min⁻¹ and dwell times of 0.5 h at the target temperature to facilitate direct comparability.

STM data were acquired at room temperature with a home-built instrument operated by a SPM 100 controller from RHK. Images were levelled and mean value filtered using the Gwyddion software. The pore geometry distributions were statistically analyzed for each molecule on both surfaces after RT deposition and after annealing to 150 °C, except for **2** on Ag(111) at RT and **1** on Cu(111) after annealing, where non-porous self-assembled and irregular covalent structures were observed, respectively. For each case at least 200 pores were evaluated and \sqrt{N} was used for the error bars.

Details of DFT simulations:

DFT simulations for isolated aggregates were performed using the Gaussian 16 software.² Therefore the '6-31+G* + LANL2DZ' mixed basis set was employed and created through the use of the 'genECP' keyword. 6-31+G* was applied to both C and H, while LANL2DZ was used to model the transition metals Ag and Cu.

Constraints were added with the 'addGIC' keyword. To assess the dependence of the total energy on the bond angle, it was necessary to freeze the C-M-C bond angle for selected values (between 180° and 165°) as well as to fix selected dihedral angles in order to impose co-planarity of the two phenyl rings in the aggregate. Apart from that, relaxation within geometry optimization was allowed.

Adsorption geometries of the debrominated and metal-terminated compound **1** were studied by periodic DFT calculations using the VASP code,³ with the projector-augmented wave method to describe ion-core interactions, and with plane waves expanded to a kinetic energy cutoff of 400 eV.

The van der Waals density functional describes exchange-correlation effects,⁴ with the version by Hamada denoted as rev-vdWDF2⁵ which has been shown to describe adsorption of molecules on coinage metals accurately.⁶ The Ag(111) and Cu(111) surfaces were modeled by four layered slabs. Furthermore, p(8×8) and p(9×9) surface unit cells were used for the calculations on Ag(111) and Cu(111), respectively, together with a 2×2 k-point sampling for both surfaces. All structures were geometrically optimized until the residual forces on all atoms (except the two bottom layers of the respective slab which were kept fixed) were smaller than 0.01 eV Å⁻¹.

Additional STM data:

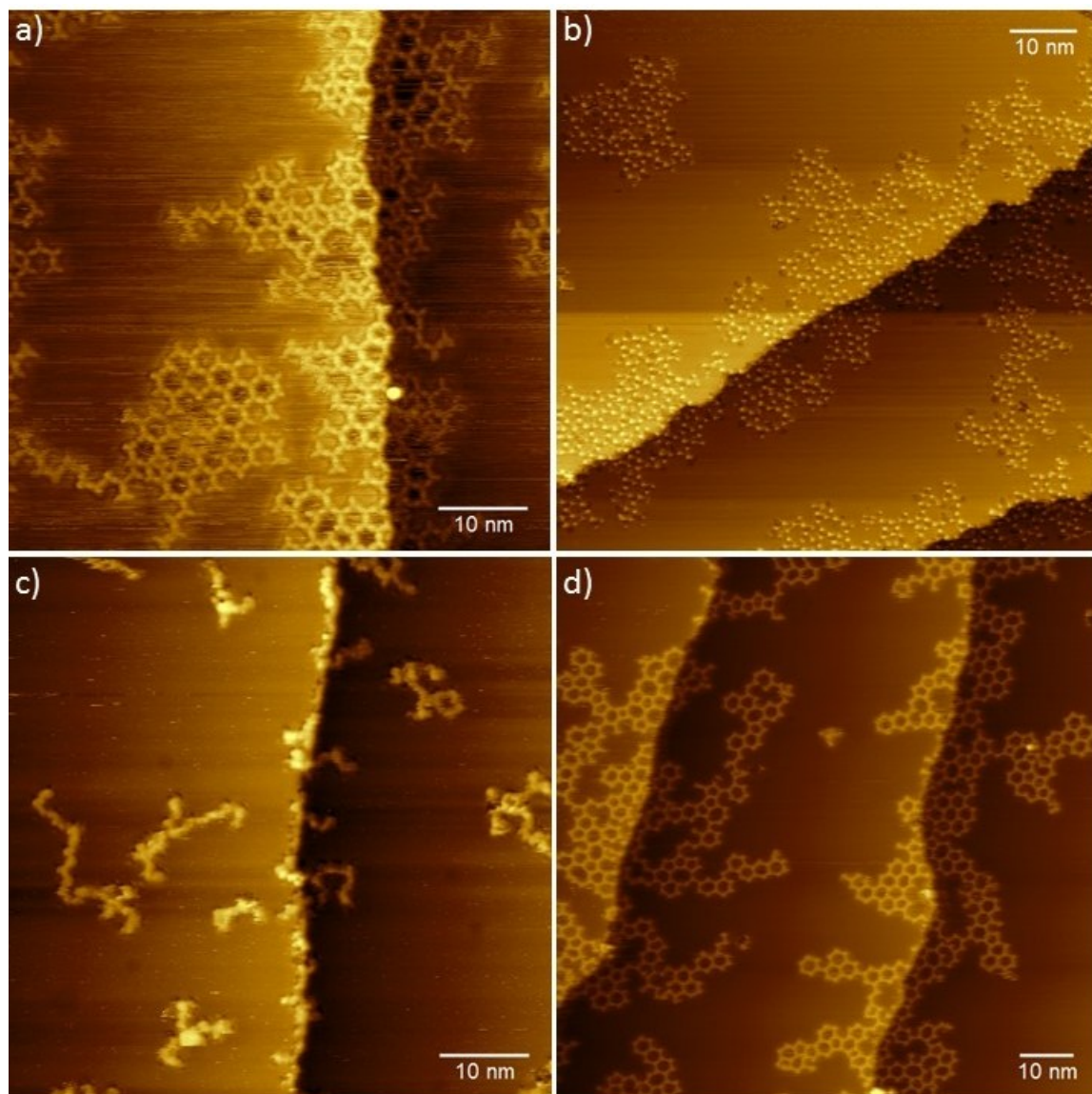


Fig. S1: Overview STM images of organometallic networks on Cu(111) complementary to Fig. 1 of the main text: (a) **1**, (b) **2** directly after RT deposition, (c) **1**, (d) **2** after annealing to 150 °C;

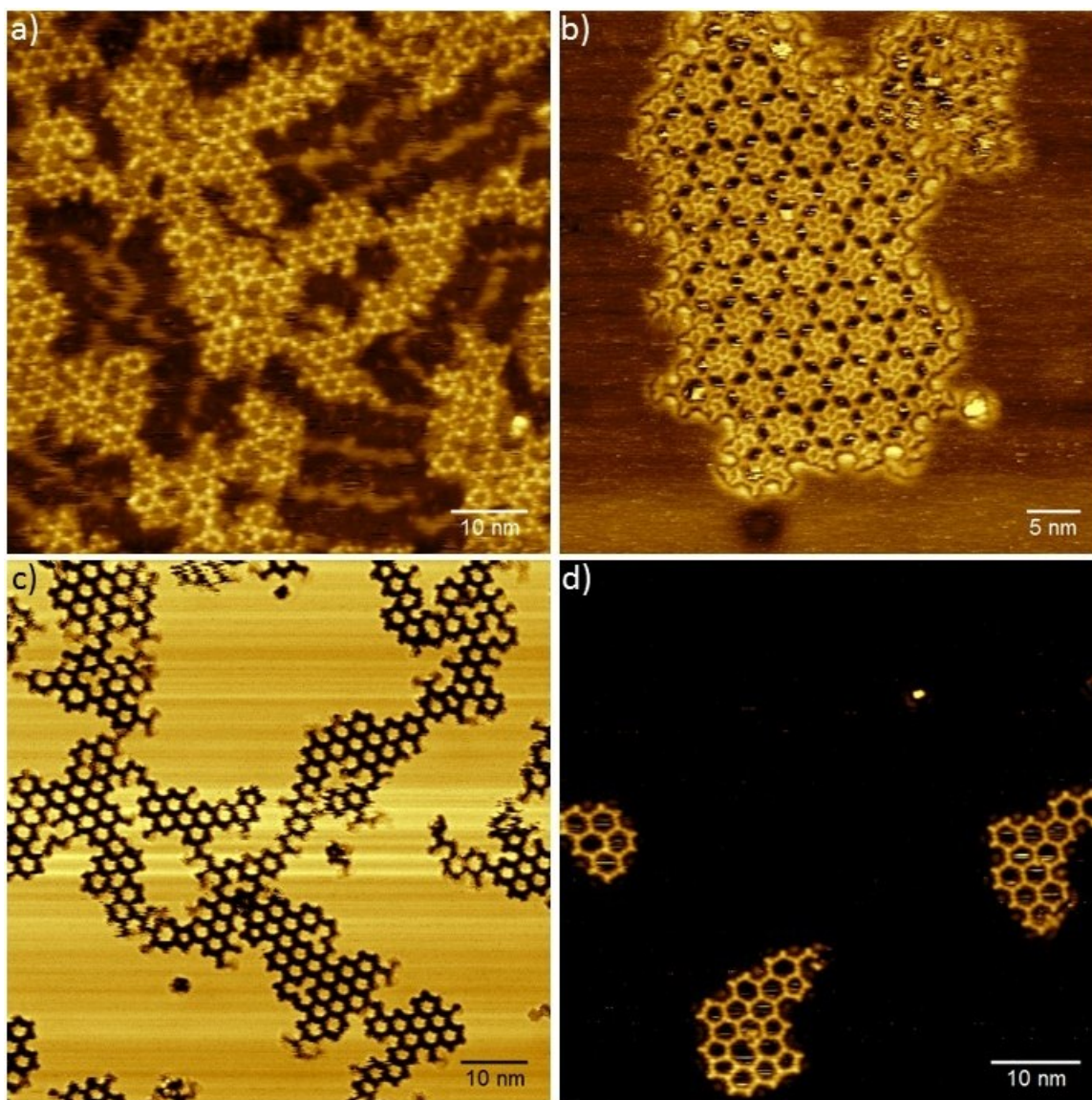


Fig. S2: Overview STM images of organometallic networks on Ag(111) complementary to Fig. 2 of the main text: (a) **1**, (b) **2** directly after RT, (c) **1**, (d) **2** after annealing to 150 °C;

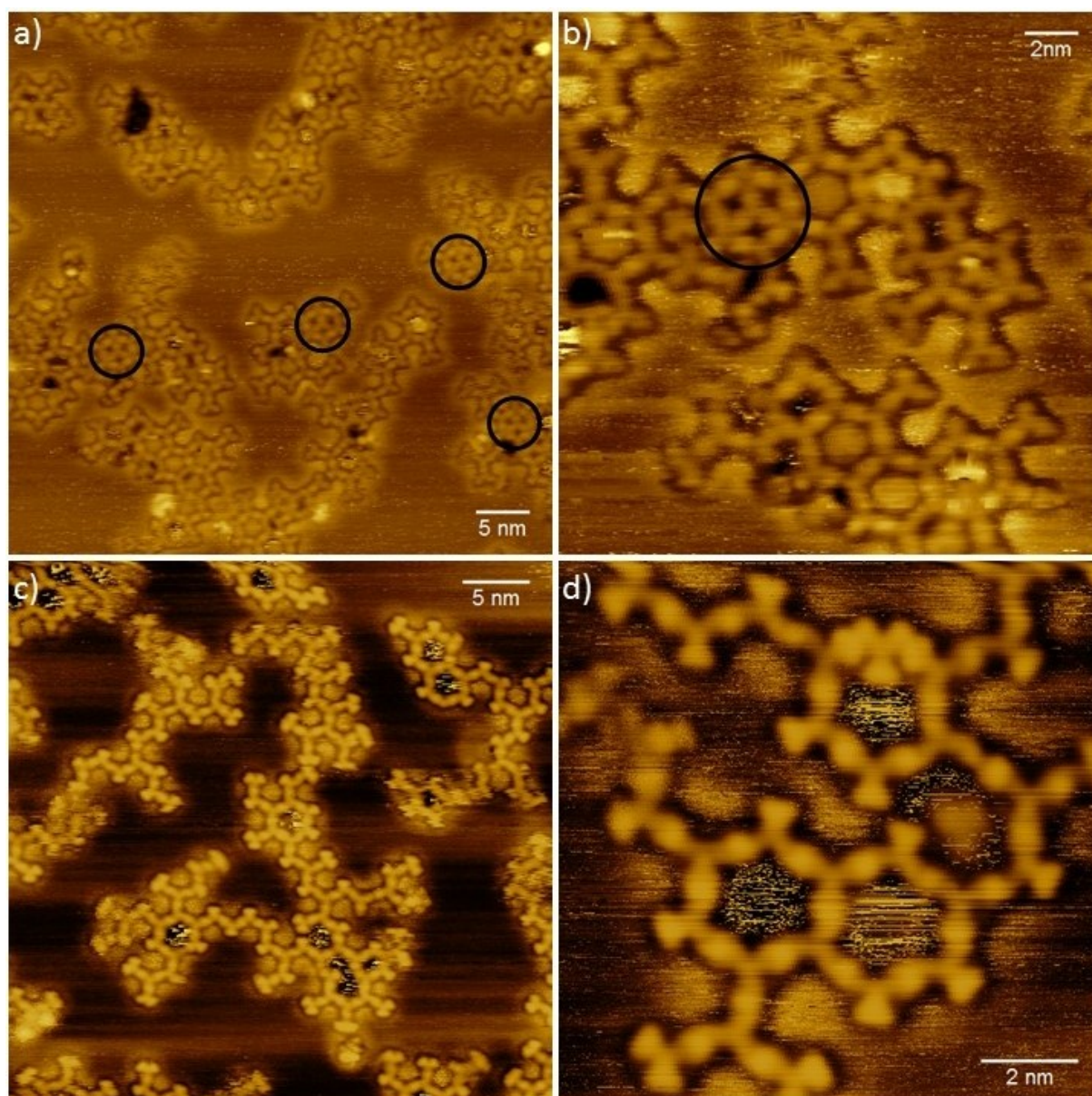


Fig. S3: STM images of organometallic networks acquired directly after (a) / (b) RT deposition of **1** onto Cu(111) and (c) / (d) after subsequent annealing to 100 °C. Additional molecules trapped inside pores (examples marked by black circles) were frequently observed after RT deposition, but could not be found anymore after annealing to 100 °C.

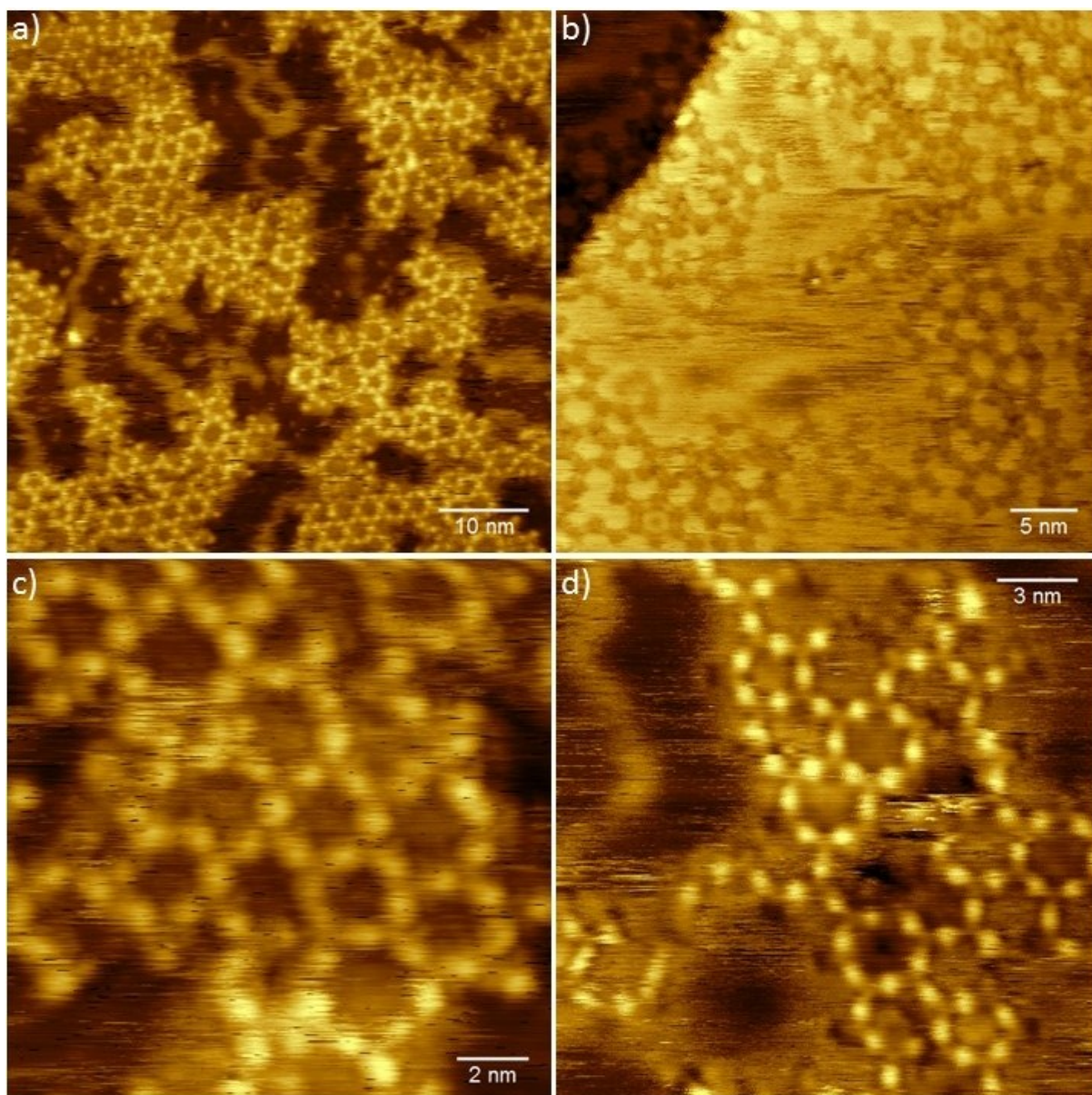


Fig. S4: STM images of organometallic networks on Ag(111): (a) **1**, (b) **2** directly after RT deposition, and (c) **1**, (d) **2** after annealing to 100 °C.

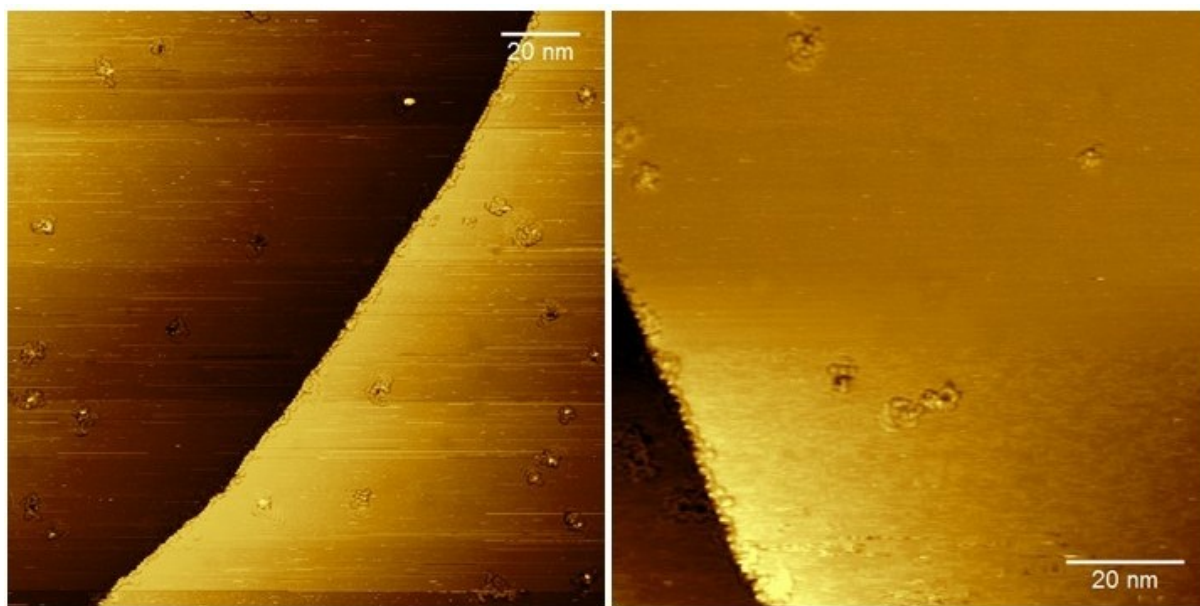


Fig. S6: STM images acquired after RT deposition of **1** onto Ag(111) and subsequent annealing to 200 °C. Most molecules desorbed from Ag(111) at higher annealing temperatures, in contrast to Cu(111), where covalent cross-linking was already observed at 150 °C.

DFT simulations of adsorption geometries on Cu(111)

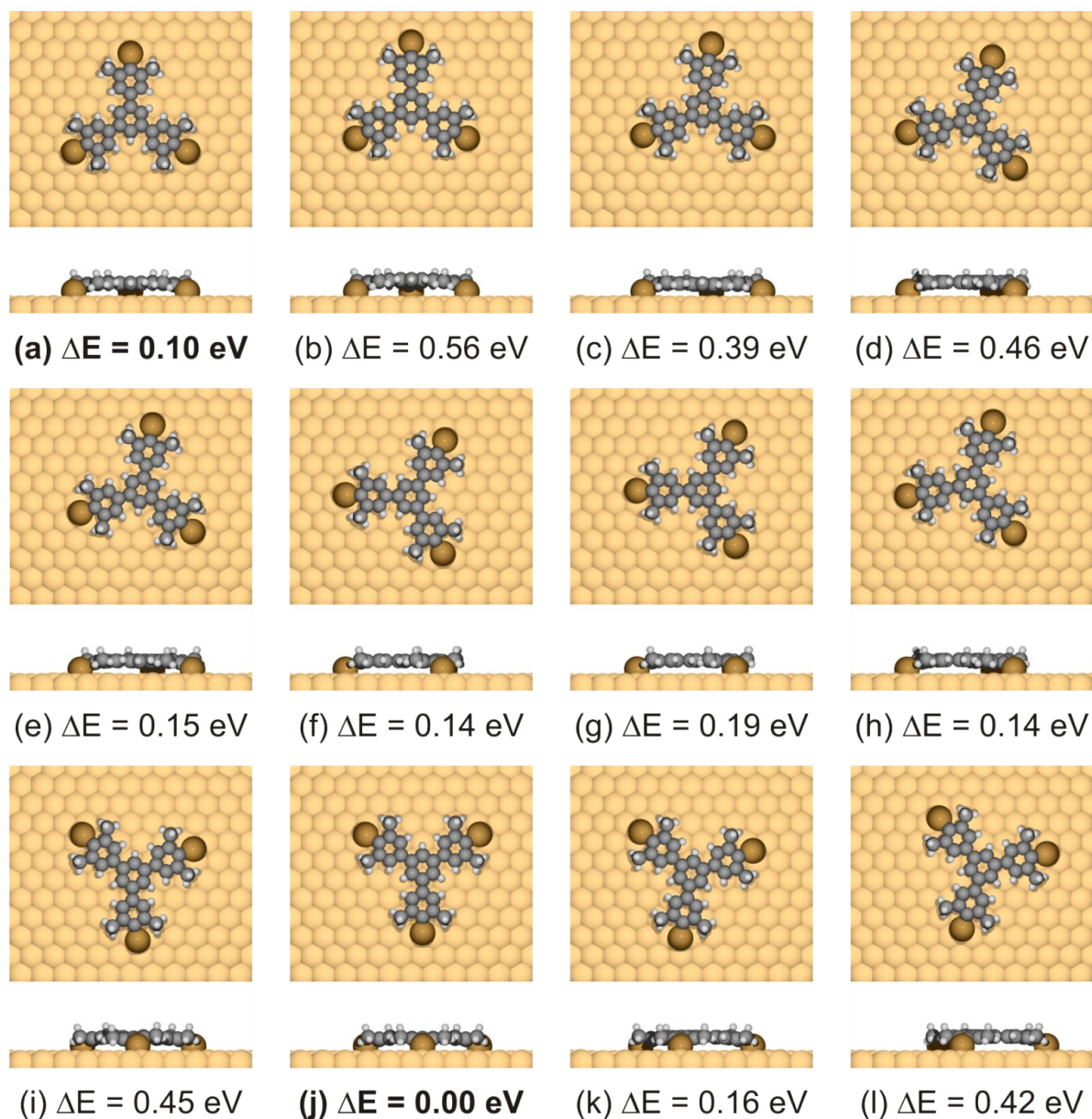


Fig. S7: Top- and side views of DFT-optimized geometries of **1** on Cu(111). All bromine substituents were replaced by Cu atoms to conform to the organometallic networks. The relative energies with respect to the most stable structure shown in (j) are given directly underneath each structure. The most stable adsorption geometry is highly symmetric: The molecule is centered above a three-fold hollow site and the mirror planes of surface and molecule are aligned. Note that the second most stable structure in (a) corresponds to the most stable structure with a 180° (or 60°) rotated molecule. These two structures are identical with respect to the topmost copper layer, but are different from the second copper layer on.

DFT simulations of adsorption geometries on Ag(111)

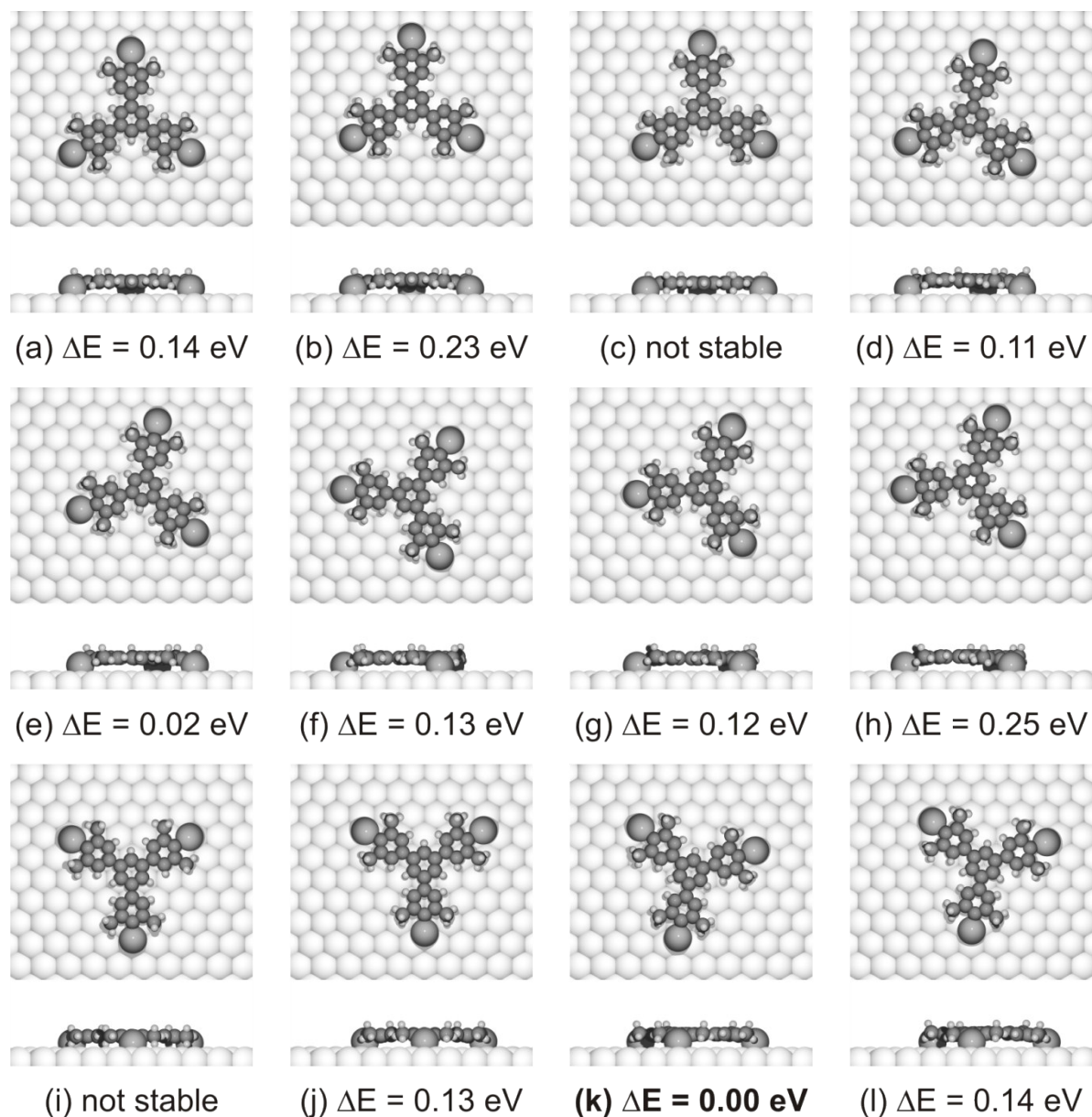
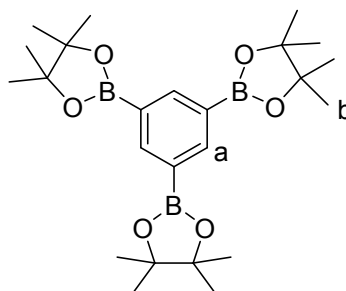


Fig. S8: Top- and side views of DFT-optimized geometries of **1** on Ag(111). All bromine substituents were replaced by Ag atoms to conform to the organometallic networks. The relative energies with respect to the most stable structure shown in (k) are given directly underneath each structure. The most stable adsorption geometry on Ag(111) is less symmetric than on that on Cu(111): The molecule is still centered above a three-fold hollow site, but the mirror planes of surface and molecule are not aligned anymore. This gives rise to two energetically equivalent adsorption geometries with a clockwise and counterclockwise rotational angle of $\sim 12^\circ$ between the mirror planes of surface and molecule. For the two unstable adsorption geometries in (c) and (i) only the respective starting geometries are shown.

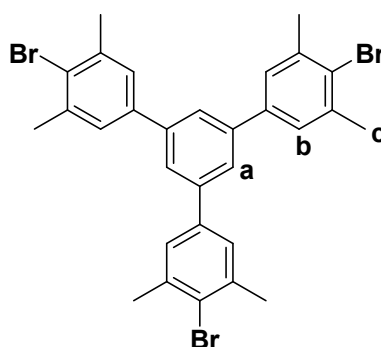
Synthesis details of 1

1,3,5-Tris(4,4,5,5-tetramethyl-1,3,2-dioxaborolan-2-yl)benzene (**3**)⁷



1,3,5-Tribromobenzene (93.0 mg, 0.295 mmol), bis(pinacolato)diboron (300 mg, 1.18 mmol), potassium acetate (434 mg, 4.43 mmol) and palladium acetate (10.0 mg, 44.0 μ mol) were combined in 15 mL of dry distilled DMF under inert atmosphere. This mixture was heated at 70 °C for 24 h maintaining inert conditions. After evaporating the solvent under vacuum, the residue was extracted with dichloromethane. The organic layer was dried over anhydrous Na_2SO_4 . The crude product was purified by column chromatography over SiO_2 (silica gel) using 5% ethyl acetate in hexane as eluent (88 mg, 65%). ^1H NMR (CDCl_3 , 400 MHz, 298 K): δ = 1.33 (s, 36H, b-H), 8.36 (s, 3H, a-H) ppm.

1,3,5-Tris(4-bromo-3,5-dimethylphenyl)benzene (**1**)



Compound **3** (80.0 mg, 0.175 mmol) and 2-bromo-5-iodo-1,3-dimethylbenzene (546 mg, 1.76 mmol) were dissolved in 25 mL of THF, 15 mL of MeOH and 10 mL of water as a solvent mixture. The solution was deoxygenated for 30 min by purging with a continuous flow of N_2 gas. Then $\text{Pd}(\text{PPh}_3)_4$ (30.3 mg, 26.3 μ mol) was added and again N_2 gas was bubbled through the solution for 10 min. After stirring the reaction mixture at 65 °C for 36 h, the organic solvents were evaporated and the aqueous part was extracted with dichloromethane. The organic layer was separated and dried over anhydrous Na_2SO_4 . Column chromatography was performed over SiO_2 (silica gel) using pentane (R_f = 0.4) as eluent to furnish the product as pure colorless solid (60 mg, 55%). Mp > 250 °C; ^1H NMR (CDCl_3 , 400 MHz, 298 K): δ = 2.51 (s, 18H, c-H), 7.37 (s, 6H, b-H), 7.67 (s, 3H, a-H) ppm; ^{13}C NMR (CDCl_3 , 100 MHz, 298 K): δ = 24.2, 125.0, 127.2, 127.3, 138.9, 139.6, 141.7 ppm; IR (KBr): ν 429, 510, 533, 570, 646, 692, 710, 734, 783, 857, 870, 883, 904, 951, 1017, 1029, 1108, 1200, 1300, 1379, 1406, 1435, 1469, 1511, 1576, 1600, 1687, 2851, 2919, 2953, 3026 cm^{-1} . Elemental Analysis: Calcd. for $\text{C}_{30}\text{H}_{27}\text{Br}_3$: C, 57.44; H, 4.34. Found: C, 57.26; H, 4.16.

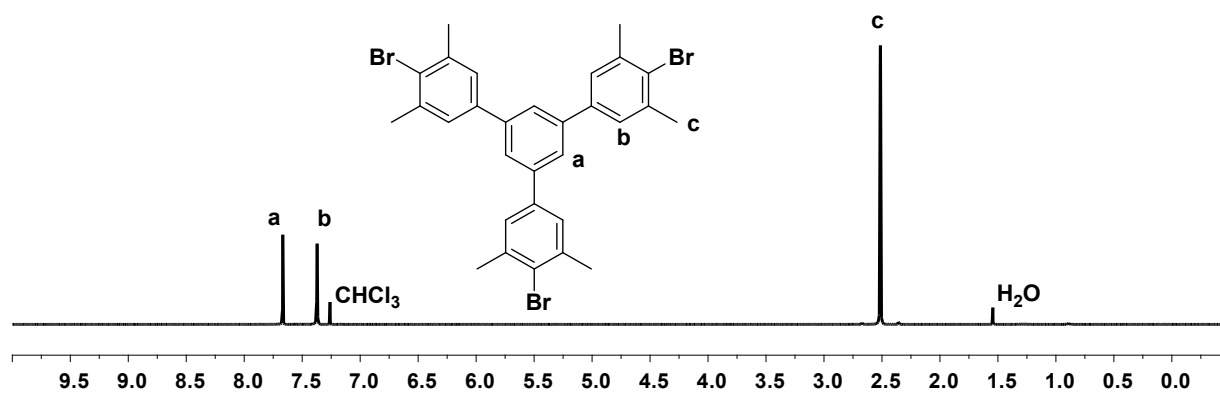


Fig. S9 ^1H NMR of compound **1** in CDCl_3 (400 MHz, 298 K).

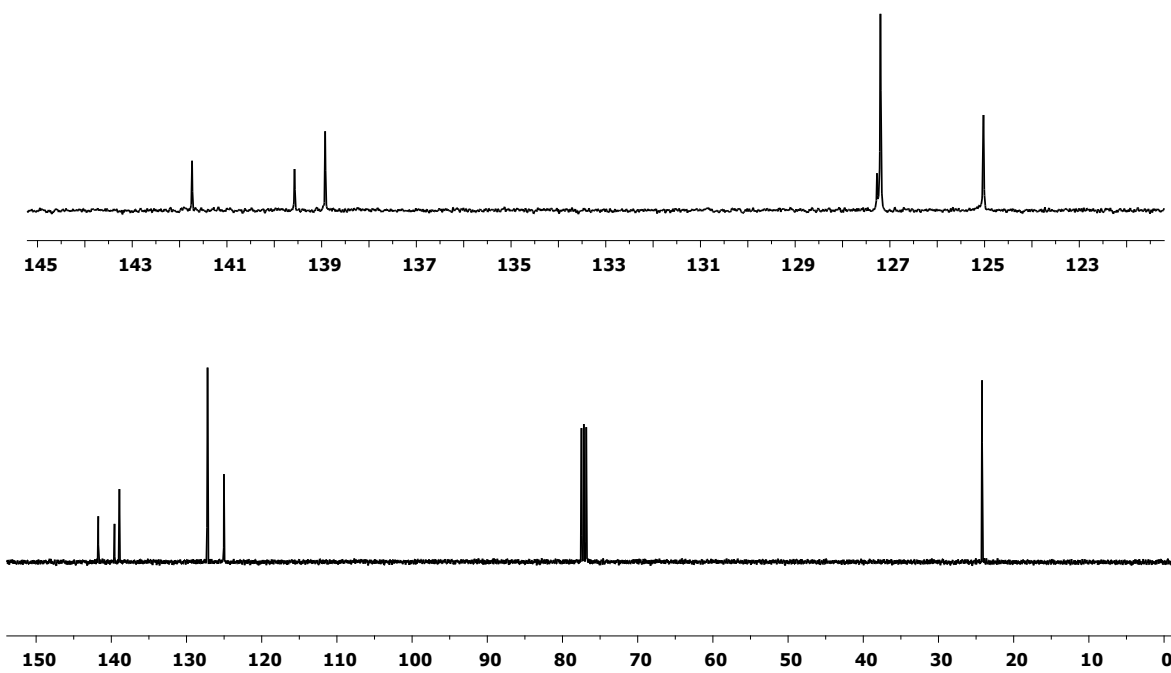


Fig. S10 ^{13}C NMR of compound **1** in CDCl_3 (100 MHz, 298 K).

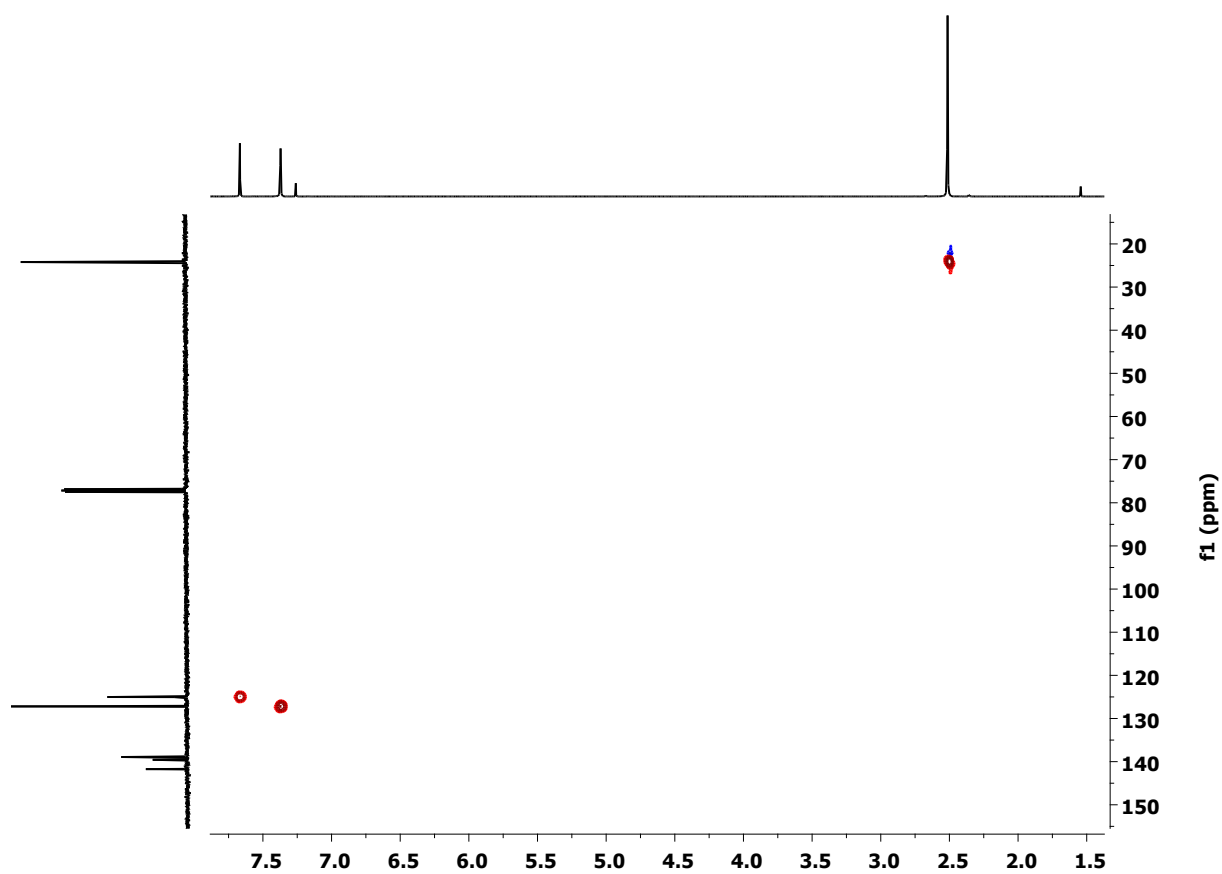


Fig. S11 ^1H - ^{13}C HSQC NMR of compound **1** in CDCl_3 (100 MHz, 298 K).

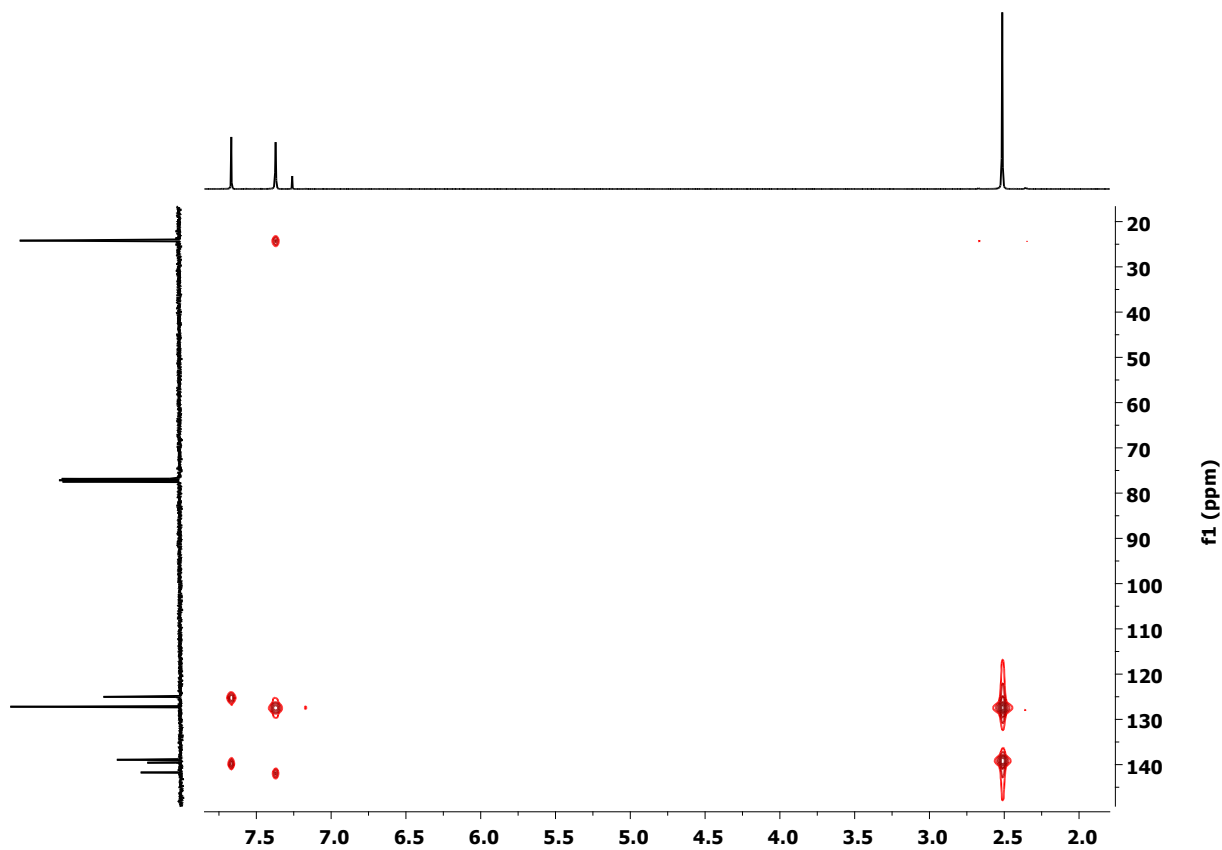


Fig. S12 ^1H - ^{13}C HMBC NMR of compound **1** in CDCl_3 (100 MHz, 298 K).

References:

1. R. Gutzler, W. M. Heckl and M. Lackinger, *Rev Sci Instrum*, 2010, **81**, 015108.
2. M. J. Frisch, G. W. Trucks, H. B. Schlegel, G. E. Scuseria, M. A. Robb, J. R. Cheeseman, G. Scalmani, V. Barone, G. A. Petersson, H. Nakatsuji, X. Li, M. Caricato, A. V. Marenich, J. Bloino, B. G. Janesko, R. Gomperts, B. Mennucci, H. P. Hratchian, J. V. Ortiz, A. F. Izmaylov, J. L. Sonnenberg, Williams, F. Ding, F. Lipparini, F. Egidi, J. Goings, B. Peng, A. Petrone, T. Henderson, D. Ranasinghe, V. G. Zakrzewski, J. Gao, N. Rega, G. Zheng, W. Liang, M. Hada, M. Ehara, K. Toyota, R. Fukuda, J. Hasegawa, M. Ishida, T. Nakajima, Y. Honda, O. Kitao, H. Nakai, T. Vreven, K. Throssell, J. A. Montgomery Jr., J. E. Peralta, F. Ogliaro, M. J. Bearpark, J. J. Heyd, E. N. Brothers, K. N. Kudin, V. N. Staroverov, T. A. Keith, R. Kobayashi, J. Normand, K. Raghavachari, A. P. Rendell, J. C. Burant, S. S. Iyengar, J. Tomasi, M. Cossi, J. M. Millam, M. Klene, C. Adamo, R. Cammi, J. W. Ochterski, R. L. Martin, K. Morokuma, O. Farkas, J. B. Foresman and D. J. Fox, *Journal*, 2016.
3. G. Kresse and J. Furthmüller, *Phys. Rev B*, 1996, **54**, 11169-11186.
4. M. Dion, H. Rydberg, E. Schroder, D. C. Langreth and B. I. Lundqvist, *Phys. Rev. Lett.*, 2004, **92**, 246401.
5. I. Hamada, *Phys. Rev B*, 2014, **89**.
6. J. Björk and S. Stafstrom, *ChemPhysChem*, 2014, **15**, 2851-2858.
7. X. Liu, Y. Xie, H. Zhao, X. Cai, H. Wu, S.-J. Su and Y. Cao, *New J. Chem.*, 2015, **39**, 8771-8779.